Soil & Environmental Health 1 (2023) 100015

Contents lists available at ScienceDirect

Soil & Environmental Health

journal homepage: www.sciencedirect.com/journal/soil-and-environmental-health

Research Paper

Biochar seeding properties affect struvite crystallization for soil application

Nageshwari Krishnamoorthy [a,b], Christopher Nzediegwu [a], Xiaohui Mao [c], Hongbo Zeng [c], Balasubramanian Paramasivan [b,**], Scott X. Chang [a,*]

[a] Department of Renewable Resources, University of Alberta, Edmonton, Alberta, T6G 2E3, Canada
[b] Department of Biotechnology & Medical Engineering, National Institute of Technology Rourkela, Odisha, 769008, India
[c] Department of Chemical and Materials Engineering, University of Alberta, Edmonton, Alberta T6G 2V4, Canada

HIGHLIGHTS

- Feedstock type and pyrolysis temperature interactively affected biochar properties.
- ~8 g L^{-1} struvite yield was obtained using sawdust biochar produced at 500 °C.
- Biochar with higher surface area and pore volume improved struvite crystallization.
- Higher hydrophobicity and biochar stability enhanced struvite crystallization.

GRAPHICAL ABSTRACT

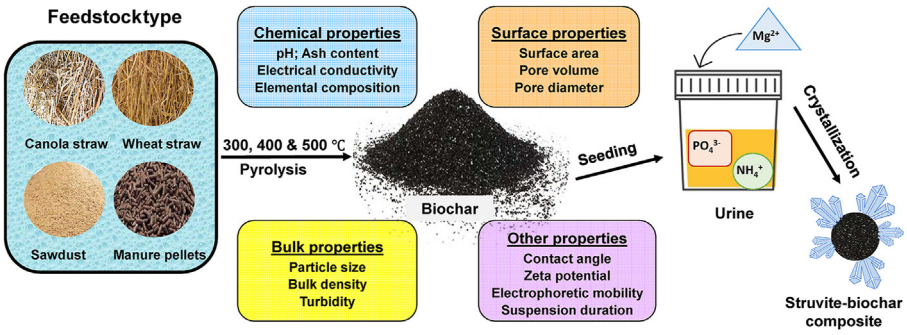

ARTICLE INFO

Handling Editor: Lena Q. Ma

Keywords:
Biochar
Microwave-assisted pyrolysis
Nucleation
Phosphorus recovery
Seeding materials
Struvite
Pyrolysis temperature

ABSTRACT

Struvite crystallization is a viable approach for recovering phosphorus from phosphorus-rich solutions such as urine and wastewater. However, designing seed materials to promote crystal growth and enhance the efficiency of struvite crystallization remains an area of active research. In this study, we investigated the seeding characteristics of biochars on struvite crystallization and the impact of biochar feedstock type and production temperature on the process. Microwave-pyrolyzed biochars produced from different feedstocks and under different temperatures were examined as seeding materials for struvite crystallization from urine and the influence of biochar properties on the overall struvite yield, nutrient recovery and struvite crystal size. Sawdust biochar (lignocellulosic biomass) produced at 500 °C had the highest struvite yield (7.91 g L^{-1}), phosphate (97.9%) and ammonium recovery (87.1%), and relative crystal size (85.2%) compared to the non-seeded treatment due to its higher surface area, pore volume, and hydrophobicity of the biochar. Manure pellet biochar (non-lignocellulosic biomass) produced at 500 °C also exhibited performance comparable to sawdust biochar produced at 500 °C. Increasing pyrolysis temperature increased biochar's hydrophobicity, zeta potential, electrophoretic mobility and bulk density, irrespective of the feedstock type, thereby improving the seeding process. The ash content of biochar was negatively correlated with its surface area, pore volume, and particle size, but positively correlated with biochar's bulk density and suspension stability. In conclusion, feedstock type and pyrolysis temperature significantly affected biochar properties, which interactively influenced struvite crystallization. Therefore, biochars should be carefully selected to improve their efficiency for phosphorus recovery from phosphorus-containing solutions such as urine and wastewater, with the recovered phosphorus being used for soil applications.

* Corresponding author.
** Corresponding author.
E-mail addresses: biobala@nitrkl.ac.in (B. Paramasivan), sxchang@ualberta.ca (S.X. Chang).

https://doi.org/10.1016/j.seh.2023.100015
Received 17 February 2023; Received in revised form 30 March 2023; Accepted 31 March 2023
Available online 6 April 2023

1. Introduction

Phosphorus (P) recovery in the form of struvite ($MgNH_4PO_4{\cdot}6H_2O$) from wastewater is emerging as a sustainable technology to reduce the adversities such as eutrophication and algal bloom (Wang et al., 2022; Nageshwari et al., 2022). Struvite is used as a fertilizer in soils because it contains some of the major nutrients (N, P and Mg) plants require and possesses slow nutrient-releasing properties (Muhmood et al., 2019; Krishnamoorthy et al., 2021). Although chemical precipitation is a simple and well-established strategy for producing struvite crystals from wastewater, only 70–80% of the P can be recovered due to the small size of struvite crystals formed. Crystal size is a critical factor in producing a stable, slow-releasing fertilizer such as struvite because it affects not only the storage, handling, and application properties but also the agronomic responses, thereby influencing nutrient uptake by plants (Tarragó et al., 2016; Wang et al., 2022). From an economic standpoint, small crystal size influences nutrient recovery and commercial scalability for fertilizer production.

Considering that struvite formation is a crystallization process, two steps including nucleation and growth mainly govern crystal development. The rate of crystallization and crystal size can be enhanced by the inclusion of seeding materials with high surface area (Zin and Kim, 2021; Nageshwari et al., 2022). The struvite crystals formed are bound to the surface of such seeding materials and serve as secondary nuclei for growth. Secondary nucleation can also occur where the irregular structures initially formed on the seed surface detach due to agitation or liquid sheer stress and serve as secondary nuclei in the bulk solution (Frawley et al., 2012). Adding seeding materials assists nucleation and can help to overcome this critical bottleneck associated with struvite crystallization.

The addition of seeding materials to wastewater has been reported to increase the struvite crystal size within a short induction time (Wang et al., 2022; Muhmood et al., 2019). However, the impact of surface properties on struvite crystallization makes finding the right seeding materials challenging. Recycled struvite fines, kaolinite, stainless steel mesh, sand, and quartz are seeding materials commonly used for nucleation. The use of struvite fines led to the production of struvite crystals with similar shapes with no phase transformation during crystal growth (Kataki et al., 2016). However, a 19% increase in struvite crystallization with struvite seeding at low P concentrations (Liu et al., 2008) and up to 75 min reduction in induction time upon supersaturation was observed (Liu et al., 2011). Yu et al. (2013) reported a 21% increase in the rate of struvite crystallization from wastewater resulting from fertilizer application and an increase in crystal size from 1.72 to 2.08 nm, when struvite was used as seed. Battistoni et al. (2000) used quartz sand to recover up to 80% phosphate as struvite, and the processing time was reduced to half. However, these materials contribute less to nutrient recovery, crystal size and nutrient value (Muhmood et al., 2019). One potential seeding material that can overcome some of the shortcomings of existing seeding materials is biochar.

Biochar is a carbonaceous product obtained by the thermochemical conversion of biomasses in oxygen-limited conditions (Nzediegwu et al., 2022; Nageshwari et al., 2022). Applying biochar for seeding struvite crystallization can improve not only the nucleation rate and crystal size but also nutrient content in biochar because it possesses a large surface area, well-developed porosity, hydrophobic surface, stability in suspension and a variety of surface functional groups (Nzediegwu et al., 2022). Biochar can act as a carrier for the nutrients in struvite, providing a slow-releasing mechanism for plant nutrient uptake over time. This can result in more efficient nutrient use and reduced leaching of nutrients into the environment. In addition, biochar contains nutrients such as P, Ca and Mg, which can increase the nutrient content of the struvite-biochar composite (Hu et al., 2019; Nageshwari et al., 2022). Biochar can improve soil structure, porosity and water-holding capacity, thereby enhancing plant nutrient availability. This can lead to improved soil health and increased crop yields. The porous structure of biochar and its cation exchange capacity can help prevent the thermodynamic hindrance of nucleation (Wang et al., 2022).

Feedstock type is one factor that influences biochar performance, and several studies have evaluated its influence on biochar struvite recovery from different wastewaters. For example, Mg-palm tree trunk biochar recovered 92.2 and 54.8% of phosphate and ammonium, respectively, from sewage sludge ash and food wastewater, while Mg-ground coffee bean biochar recovered 79.5 and 38.6%, respectively. Higher recovery by Mg-palm tree trunk biochar corresponded with its larger surface area and porous nature (Zin and Kim, 2021). Wheat straw and rice husk biochars similarly increased struvite particle size, phosphate and ammonium recovery by 43, 7 and 11%, respectively, from an anaerobic digestate supernatant. Wheat straw showed higher nutrient recovery due to higher surface area and porosity (Muhmood et al., 2019). The effects of producing biochars from various feedstocks and at different temperatures on struvite recovery from urine are not well understood; hence, evaluating such impacts on struvite recovery from urine using biochar is crucial because urine contributes 90% phosphate and 70% nitrogen load to municipal wastewater (Krishnamoorthy et al., 2021).

Therefore, the objectives of the current study were to: 1) evaluate the effect of feedstock type and pyrolysis temperature on biochar's nucleation properties; 2) analyze the influence of biochar's nucleation properties on struvite yield, phosphate and ammonium recovery and relative crystal size; and 3) understand the individual and interactive effects of biochar's nucleation properties on struvite crystallization. This study will offer new data on the utility of different biochars on P recovery from *P*-rich solutions.

2. Materials and methods

2.1. Biochar production

Three lignocellulosic feedstocks, including canola straw (CS), wheat straw (WS), and sawdust (SD) of white spruce were locally sourced in Alberta, Canada. A non-lignocellulosic biomass, manure pellet (MP), was obtained from Paragon Soil and Environmental Consulting Inc., Edmonton, Alberta, Canada. The details of feedstock collection and pretreatment can be found in Kwak et al. (2019). For biochar production, the feedstocks were oven-dried at 60 °C for 24 h, loaded at half capacity in a 900 mL quartz reactor vessel, which was pyrolyzed at 300, 400 and 500 °C in a BP-091 microwave oven (Microwave Research and Application Inc., Carol Stream, IL) operated at 2.45 GHz. The 300, 400 and 500 °C represent low, medium, and high temperatures, respectively (Foong et al., 2020; Huang et al., 2015). Further details on biochar production process can be found in Nzediegwu et al. (2021). After pyrolysis, the biochars were cooled to ~25 °C and stored in an air-tight bag. The samples were named as CS300, CS400, CS500, WS300, WS400, WS500, SD300, SD400, SD500, MP300, MP400 and MP500, based on the feedstock type and pyrolysis temperature. The yield (%) of microwave-assisted pyrolysis (MAP) process was calculated using Eq. (1).

$$Yield = \frac{Mass\ of\ biochar\ (g)}{Mass\ of\ feedstock\ (g)} * 100 \quad (1)$$

2.2. Synthetic urine preparation

The synthetic urine was prepared as per the *P*-urine composition reported by Liao et al. (2020) (Table S1). The pH of synthetic urine was maintained at 9.0 ± 0.2 using 1 M NaOH and 1 M HCl. The urine was completely sealed for storage to avoid loss of ammonia. The method for estimation of biochar pH in NaCl used by Fidel et al. (2017) was modified by replacing synthetic urine in place of NaCl for studying the variation in urine pH with respect to the addition of biochar. Biochar was added at 1 g L^{-1} to the urine, and the pH was measured using a pH meter (Thermo Fisher Scientific Inc., Beverly, MA). The change in pH was noted for every 5 min interval. The synthetic urine sample without biochar was

maintained as the control. Change in the pH of synthetic urine was considered to have a direct effect on struvite crystallization. The treatments were replicated three times.

2.3. Biochar characterization

The biochar samples were ground to fine particles using a ball mill (MM200, Retsch GmbH, Haan, Germany) and sieved through a 425 μm sieve for further analysis. Please see Nzediegwu et al. (2021) for details on size reduction.

Physicochemical properties: The pH of the biochar samples was measured in a supernatant created by equilibrating biochar in deionized water (1: 10 w:v) for 1 h (Fidel et al., 2017). The electrical conductivity of the biochar particles suspended in deionized water (0.5 g L^{-1}) was measured using a Zetasizer Nano ZSP device (Malvern, UK). The ultimate analysis and ash content data of the biochars were adapted from Nzediegwu et al. (2021).

Surface properties: The Brunauer–Emmet–Teller (BET) specific surface area, pore volume, and pore diameter of biochars were determined using an Autosorb 1 MP surface area analyzer by N_2 adsorption at 77 K (Quantachrome Instruments, Boynton Beach, FL) after the samples (~200 mg) were degassed at 120 °C for 2 h.

Bulk properties: The bulk density of biochars was determined as per Stella Mary et al. (2016), where the samples were filled up to a certain volume in a measuring cylinder and oven-dried at 80 °C overnight. The cylinder was then tapped for a few minutes to ensure the compactness of the chars. The bulk density of the biochar was calculated using Eq. (2).

$$Bulk\ density\ \left(g\ cm^{-3}\right) = \frac{Dry\ weight\ of biochar\ (g)}{Volume\ of\ packed\ biochar\ (cm^3)} \quad (2)$$

The turbidity of the biochar-suspended solution (0.5 g L^{-1}) was measured as a secondary parameter to assess the density using a turbidity meter (LaMotte, 2020t/I, USA), and the same solution was used to measure the biochar particle size using a Zetasizer Nano ZSP (Malvern, UK).

Suspension properties: Biochars' hydrophobicity was studied using the O/C ratio and contact angle method. The contact angle measurements were performed by sessile drop technique at room temperature using a Ramé-Hart contact angle goniometer, USA. The biochar samples were fixed on a glass slide using double-sided adhesive tape to prevent movement of the water droplet (5 μL) on the flat surface during wetting. The measurements were recorded based on the shape of the sessile drop as imaged by the goniometer and repeated at least three times for each sample.

The electrokinetic properties of biochar, such as zeta potential and electrophoretic mobility, were analyzed using a Zetasizer Nano ZSP (Malvern, UK) in a suspension formed by equilibrating biochar in deionized water (0.5 g L^{-1}) for 12 h. The suspension duration of the biochar particles in water was monitored and noted.

2.4. Struvite crystallization experiments

Struvite crystallization experiments were conducted for the biochars produced from different feedstocks and at different temperatures to optimize the biochar type appropriate for seeding struvite crystallization. $MgCl_2.6H_2O$ procured from Fisher Scientific Co. was used as the source of magnesium for struvite formation. To optimize the most suitable biochar type, $MgCl_2{\cdot}6H_2O$ was added to the synthetic urine in a 1: 1 (Mg^{2+}: PO_4^{3-}) ratio followed by the biochar samples in a 1 g L^{-1} dosage. The solution was stirred for 30 min for effective nucleation and dispersion of magnesium. The supernatant was decanted and stored after a retention time of 8 h, and the struvite-biochar composites precipitated at the bottom were collected and oven-dried at 40 °C overnight and stored in Ziploc bags. The biochar type for seeding was optimized based on the outcomes of phosphate and ammonium recovery, struvite yield, and crystal size. The control samples without biochar addition were the non-seeded treatment. The phosphate (PO_4^{3-}) concentration was analyzed by the ascorbic acid-molybdenum blue method reported by Murphy and Riley (1962). The ammonium (NH_4^+) concentration was colorimetrically determined with Iodophenol blue method at 636 nm absorbance. Before and after struvite precipitation, the PO_4^{3-} and NH_4^+ concentrations in synthetic urine were measured using a spectrophotometer (Genesys™ 10 series, Thermo Electron Scientific Instrument Corporation, USA), and the recovery was calculated using Eqs. (3) and (4), respectively (Krishnamoorthy et al., 2020). The struvite yield was calculated by subtracting the amount of biochar added from the total weight of the struvite-biochar composite. The struvite crystal size after seeding was analyzed with Zetasizer Nano ZSP (Malvern, UK), and the relative percentage difference in size with respect to struvite crystals obtained from control was calculated using Eq. (5).

$$PO_4^{3-}\ recovery\ (\%) = \frac{PO_4^{3-}Inital - PO_4^{3-}Final}{PO_4^{3-}Initial} \times 100 \quad (3)$$

$$NH_4^{+}\ recovery\ (\%) = \frac{NH_4^{+}Inital - NH_4^{+}Final}{NH_4^{+}Initial} \times 100 \quad (4)$$

Where, $PO_4^{3-}Inital$ and $NH_4^{+}Inital$ are the initial concentrations of phosphate and ammonium, respectively, and $PO_4^{3-}Final$ and $NH_4^{+}Final$ are the final concentrations of phosphate and ammonium, respectively.

$$Relative\ percentage\ difference\ (\%) = \frac{CS_A - CS_C}{\frac{CS_A + CS_C}{2}} \times 100 \quad (5)$$

where, CS_A and CS_C are struvite crystal size after seeding with the biochar and control treatments, respectively.

Once the biochar type was optimized, the optimum dosage was determined by varying the biochar concentrations to 0.5, 1, 1.5 and 2 g L^{-1} of synthetic urine. The Mg concentration, reaction and retention time and drying conditions were maintained the same as in the previous optimization step. The final optimized char sample was stored for further characterization and analysis. All the optimization experiments were conducted in triplicates.

2.5. Statistical analysis

The struvite yield and phosphate and ammonium recovery data were subjected to a one-way analysis of variance in Origin Pro to analyze the effect of biochar seeding on struvite crystallization. When the treatment was significant ($p < 0.05$), the Tukey post hoc test was performed to compare the means. The linear relationship between the biochar properties and struvite crystallization properties regarding feedstock type and pyrolysis temperature was studied using the Pearson correlation matrix. The Pearson coefficients were calculated using the *scipy* package in Python, and the plots were generated using the *seaborn* package. The relationship between the biochar properties and their contribution to struvite crystallization was determined from the correlation centroid and biplots obtained from PCA using XLSTAT version 2021.January 3, 1149 statistical software.

3. Results and discussions

3.1. Feedstock type and pyrolysis temperature affect biochar properties

pH is a crucial parameter that determines struvite formation. An alkaline pH (7–11.5) favors struvite precipitation or prevents its solubilization (Krishnamoorthy et al., 2020, 2021). In an ideal scenario, adding biochar to any liquid medium should alter its pH. However, the change in synthetic urine pH was negligible for the biochars used in this work (data not shown). This could be because of the high phosphate concentration in urine that acts as a buffer to stabilize pH (Prabhu et al., 2021). Therefore, biochar's pH should not affect struvite crystallization.

An increase in EC is beneficial for struvite crystallization. In the case of urine, the process of ureolysis (breakdown of urea to ammonia/ammonium and carbon dioxide) increases the solution EC and pH (Krishnamoorthy et al., 2020). For lignocellulosic biomass-derived biochars, EC was highest for canola straw and lowest for sawdust (Table 1). However, in the case of manure pellet, higher ash did not contribute to EC, which could be due to fewer water-soluble minerals. For a given feedstock, the EC increased with an increase in pyrolytic temperature, similar to the findings of Ghabi et al. (2020).

Biochar with a higher surface area can not only act as a good adsorbent/seed material but also help in the retention and sustained release of ions from struvite when applied in the soil. The surface area of biochars ranged from 1.5 $m^2\ g^{-1}$ for CS300 to 43 $m^2\ g^{-1}$ for SD500 (Table 1). The values are comparable to MAP-derived biochars from organic wastes such as sludge, algae, pine wood, and corn stalk (Zhang et al., 2022). The pore volume of biochars was consistent with surface area, varying from 0.0008 $cm^3\ g^{-1}$ for CS300 to 0.0273 $cm^3\ g^{-1}$ for SD500 (Table 1). While the pore diameter was highest for SD500 (22.5 Å), it was lowest for CS500 (14.2 Å) (Fig. S1). The volumetric heating mechanism in MAP makes tar vaporization faster, leading to the development of micropores in biochar (Wallace et al., 2019). Theoretically, surface area and pore volume increase with increasing the pyrolytic temperature due to the removal of water and other volatile organic matter in the form of O and H and the expansion of pores due to the flow of gaseous products generated (Zhang et al., 2022). However, fluctuations can be observed in all biochars, except for wheat straw, due to complex condensation and devolatilization of volatiles or closure of pores because of sintering occurring above the critical temperature (Nzediegwu et al., 2021). Another plausible reason could be the formation of hotspots due to microwave heating, which could cause variables in the surface characteristics of biochar. Such inconsistencies were observed by Huang et al. (2015) where the specific surface area decreased with an increase in MAP temperature beyond 300 °C.

The particle size of biochar or struvite in a soil determines their agronomic effects on the soil, where larger particles have longer effects. The average particle size (Z-average) of biochar varied from 1.36 μm (MP500) to 5.14 μm (CS300) (Fig. 1a). The difference in the relative struvite crystal size upon seeding was determined with respect to the size of struvite crystals formed in the control experiments (3.56 ± 1.32 μm) (Fig. 1b). All biochars increased struvite crystal size, despite their varied particle size. The contribution of particle size alone towards seeding has not been discussed extensively in the literature. In this study, SD500 offered the highest relative crystal difference of 85.1%. This is much higher than the results of Muhmood et al. (2019), where a 43% increase in crystal size with biochar seeding was obtained.

Biochar decreases the bulk density of soil, which is desirable for water and air movement. In the case of crystallization, the biochar's bulk density indicates the number of seed particles loaded into the solution. Due to their high ash content, bulk densities were the highest for manure pellet biochars. The wheat straw and sawdust biochars share the lowest bulk densities, corresponding to their ash content and pore volume. The bulk density of every feedstock increased with pyrolysis temperature due to the development of porous structures because of volatilization and loss of organic constituents (Fig. 1c). Similar results were obtained by Claoston et al. (2014) when biochars were produced from empty fruit bunch and rice husk at pyrolysis temperatures between 350 and 650 °C. Turbidity, on the other hand, is inversely proportional to the bulk density of biochar (Fig. 1d).

Hydrophobicity is the water-repelling characteristic of biochar and affects the water holding capacity of the soil (Adhikari et al., 2022). For crystallization, the seed material is required to remain in suspension for effective nucleation and is expected to have optimum hydrophobicity. The contact angle was used as a measure of hydrophobicity in the current study. Irrespective of the feedstock type, the contact angle (hydrophobicity) increased with pyrolysis temperature (Table 2), due to the presence of alkyl and aromatic groups present on the surface of biochar and the loss of O-containing groups during pyrolysis (Hassan et al., 2020). Hydrophobicity is also affected by various indirect factors of biochar, such as O/C ratio, alkalinity, surface area, pore volume, particle size, and the type and abundance of surface functional groups. The O/C ratio is indirectly correlated with hydrophobicity, as a low O/C ratio indicates the presence of aromatic compounds (Hassan et al., 2020). In this study, the O/C ratio declined with increased pyrolysis temperature for a given feedstock type. WS500 was the only biochar with superhydrophobic nature with a water contact angle of 153° and O/C ratio of 0.07. Such strongly hydrophobic biochars (>135°) were unsuitable for crystallization, as the particles floated on the surface of the reaction fluid medium without participating in nucleation. On the other hand, slightly hydrophobic biochars (100–120°) with relatively larger particle sizes settled at the bottom. Though a minimum mixing duration was opted to assist nucleation, such critical conditions require higher mixing to enable the particles to participate, which might add to the cost.

The zeta potential values seem to have increased for the samples prepared above 300 °C for all feedstocks except for manure pellets (slight decrease). Biochars tend to have a negative surface charge due to their O-containing functional groups as influenced by feedstock type and pyrolysis temperature. The biochars' high magnitude of zeta potential depicts higher colloidal stability (prevents metal mobilization in a soil) due to the electrical double-layer repulsion, which is more suitable for nucleation (Xu et al., 2020). The zeta potential of suspended particles is affected by the aqueous media's pH, EC and salinity. Zeta potential and electrophoretic mobility are interrelated and can be derived from one another using the Smoluchowski equation (Xu et al., 2020). Higher pyrolysis temperatures resulted in higher magnitude, portraying a higher velocity of biochar in the aqueous medium as conducive for nucleation.

Table 1
Physicochemical properties of biochars produced from various feedstocks at different pyrolysis temperatures (pH and electrical conductivity data are summerized as mean ± standard deviation).

Feedstock	Production temperature (°C)	pH	Electrical conductivity (μS cm^{-1})	Surface area ($m^2\ g^{-1}$)[a]	Pore volume ($cm^3\ g^{-1}$)
Canola straw	300	7.02 ± 0.05	168.00 ± 2.00	1.5	0.0008
	400	7.34 ± 0.04	198.66 ± 2.51	4.3	0.0026
	500	9.27 ± 0.07	202.00 ± 2.00	3.2	0.0012
Wheat straw	300	6.67 ± 0.06	67.43 ± 0.80	3.9	0.0023
	400	8.47 ± 0.05	72.53 ± 1.70	4.9	0.0025
	500	8.67 ± 0.04	83.40 ± 1.11	4.8	0.0026
Sawdust	300	6.71 ± 0.05	4.75 ± 0.15	5.2	0.0035
	400	6.73 ± 0.04	4.99 ± 0.58	1.7	0.0009
	500	7.17 ± 0.06	12.45 ± 11.19	43.0	0.0273
Manure pellet	300	7.22 ± 0.02	63.96 ± 1.25	4.5	0.0022
	400	7.47 ± 0.06	67.63 ± 1.05	3.4	0.0009
	500	7.64 ± 0.03	72.53 ± 0.75	9.7	0.0051

[a] Data adapted from Nzediegwu et al. (2021).

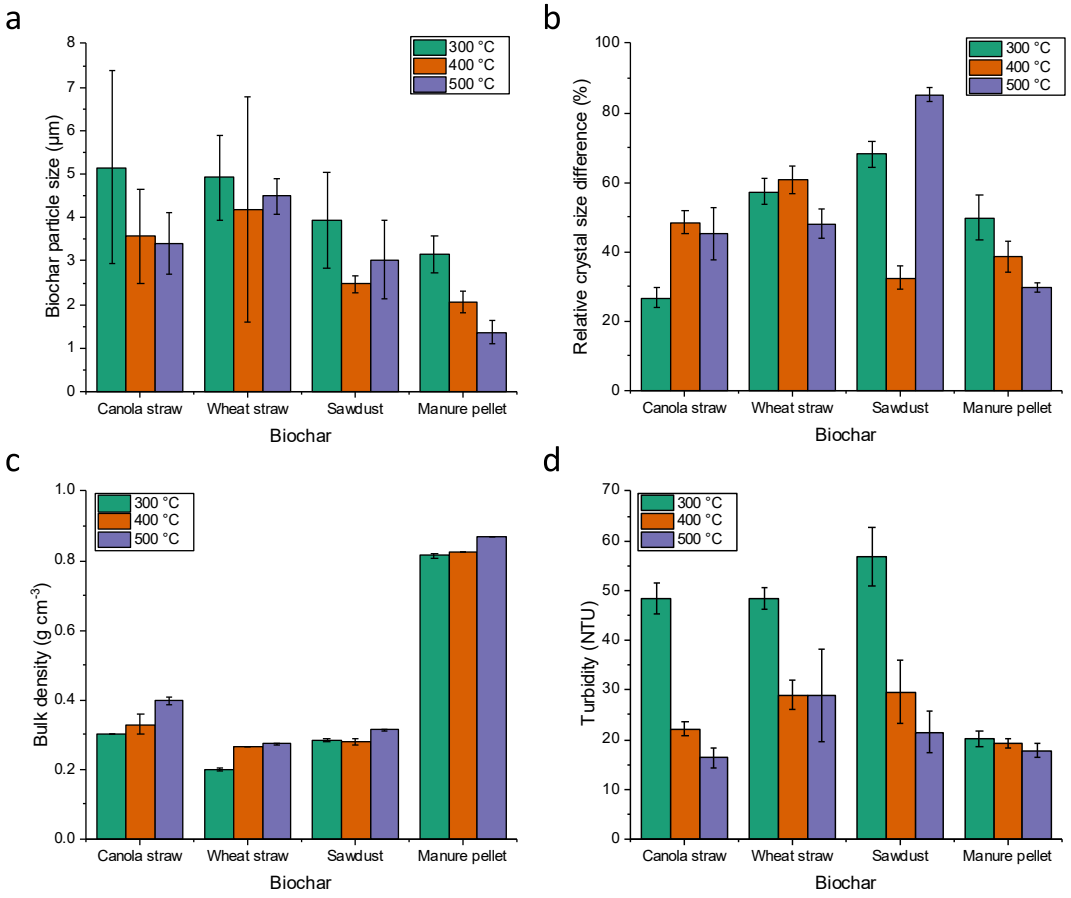

Fig. 1. Effects of feedstock type and pyrolysis temperature effects on a) Particle size of biochars and b) Relative struvite crystal size difference with seeding and c) Bulk density of biochars and d) Turbidity of biochars in solution (error bars represent standard deviation).

Table 2
Suspension properties of biochars produced from various feedstocks at different pyrolysis temperatures (Data are summerized as mean ± standard deviation).

Feedstock	Production temperature (°C)	Contact angle (°)	O/C ratio[a]	Zeta potential (mV)	Electrophoretic mobility (μm Cm Vs^{-1})
Canola straw	300	124 ± 4	0.28 ± 0.00	−19.96 ± 3.45	−1.56 ± 0.26
	400	133 ± 8	0.13 ± 0.00	−27.36 ± 0.57	−2.14 ± 0.04
	500	136 ± 4	0.10 ± 0.00	−30.76 ± 0.35	−2.41 ± 0.02
Wheat straw	300	122 ± 2	0.24 ± 0.01	−37.10 ± 0.98	−2.91 ± 0.07
	400	130 ± 4	0.13 ± 0.00	−46.83 ± 1.00	−3.67 ± 0.07
	500	152 ± 4	0.07 ± 0.00	−52.70 ± 2.60	−4.12 ± .020
Sawdust	300	98 ± 7	0.35 ± 0.01	−6.02 ± 2.90	−0.47 ± 0.16
	400	111 ± 5	0.15 ± 0.00	−20.90 ± 9.26	−1.63 ± 0.72
	500	124 ± 8	0.09 ± 0.00	−28.46 ± 1.77	−2.23 ± 0.14
Manure pellet	300	116 ± 3	0.22 ± 0.14	−18.03 ± 0.51	−1.41 ± 0.04
	400	120 ± 7	0.23 ± 0.11	−17.70 ± 0.26	−1.38 ± 0.01
	500	135 ± 3	0.12 ± 0.05	−19.83 ± 1.26	−1.55 ± 0.09

[a] Adapted from Nzediegwu et al. (2021).

3.2. Optimization of biochar type and dosage for struvite crystallization

The biochar type and dosage were optimized based on three outcomes of struvite crystallization: struvite yield, phosphate, and ammonium recovery. There was a substantial increase in yield for all biochar-seeded struvite samples compared to the control (non-seeded treatment) (Fig. 2). SD500 biochar offered the highest struvite yield (7.91 g L^{-1}), followed by MP500 (7.29 g L^{-1}). The yield values obtained in this study were high compared to the control (4.07 g L^{-1}) and other non-seeded struvite treatment results (Robinson Junior et al., 2022; Krishnamoorthy et al., 2020). Wang et al. (2022) recorded a comparable struvite yield when seeded with mealworm frass biochar (7.50 g L^{-1}). The reason behind SD500 outperforming other biochars could be its higher surface area and pore volume. These two parameters were reported to be the most essential in seeding or any adsorption-related studies (Muhmood et al., 2019). In addition, several other biochar properties discussed earlier could have contributed to struvite recovery, which also explains the difference in performance between biochars.

Compared to the control, phosphate recovery was increased with the addition of all biochar samples, except for WS500 seeded struvite, for which the recovery was almost the same as the control (80.4%). SD500 offered the highest phosphate recovery of 97.8%, followed by MP500 (93.7%). Similar results were obtained by Muhmood et al. (2019) and Zin and Kim, (2021), where biochars were used to seed struvite crystallization. In a pilot scale study, mealworm frass biochar recovered 96.1% phosphate as struvite from refuse transfer station leachate, along with 42.1% chemical oxygen demand removal (Wang et al., 2022). Analysis was carried out to estimate inherent phosphate leaching from biochar as these ions could

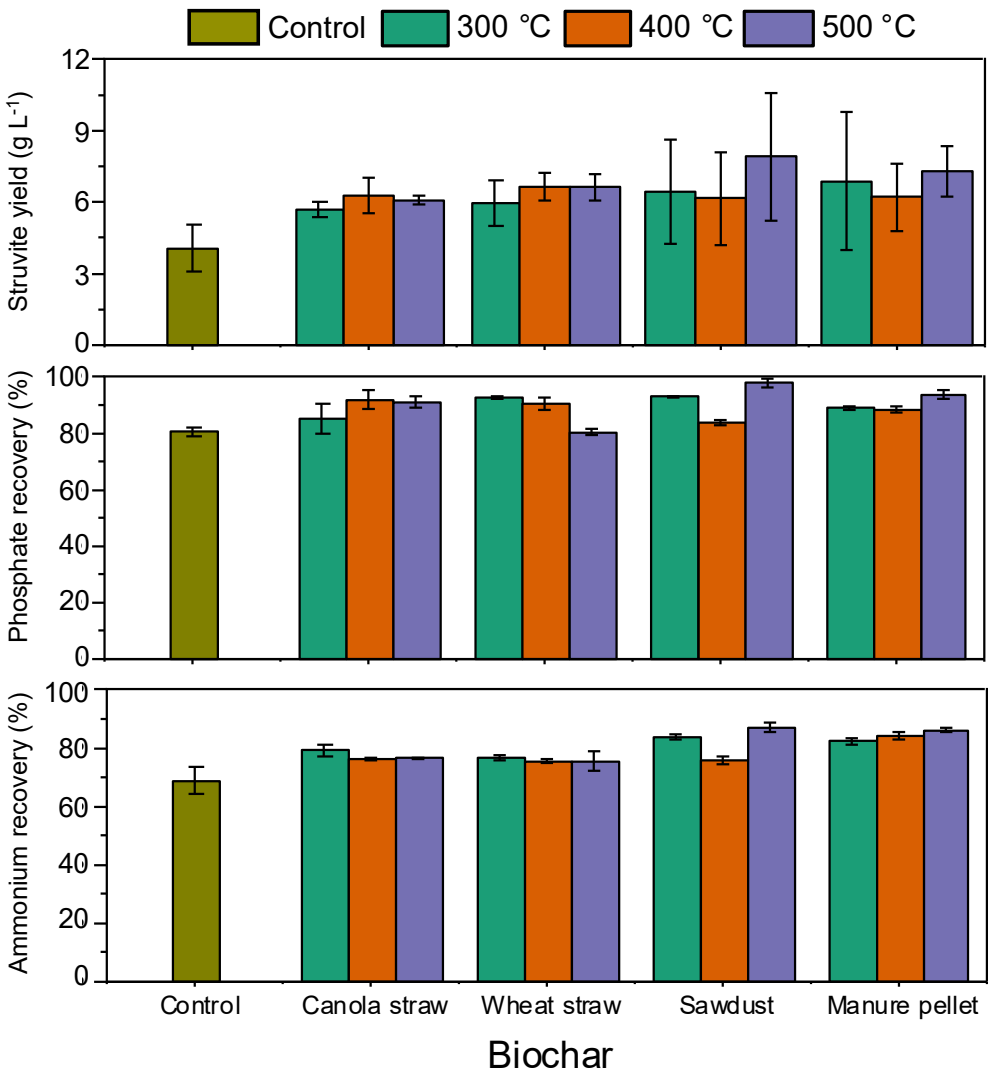

Fig. 2. Struvite yield, phosphate, and ammonium recovery with respect to the addition of biochar produced from various feedstocks at different pyrolysis temperatures (error bars represent standard deviation, and both feedstock type and pyrolysis temperature significantly affected phosphate and ammonium recovery).

also participate in struvite formation. It was observed that the phosphate released into the medium was negligible (<1 mg L^{-1}) for biochars produced from all feedstocks (Fig. S2). Among the biochars, manure pellet and sawdust had the highest and least phosphate leach, respectively, corresponding with their inorganic constituents (ash content) present. A decline in leach with an increase in pyrolysis temperature for all feedstocks can also be seen in Fig. S2. Similar conclusions reporting phosphorus retention in biochar with temperature due to the transformation of soluble phosphorus into more stable forms, regardless of the feedstock, can be seen in the literature (Chen et al., 2020; Xu et al., 2016).

The addition of biochar seeds improved the ammonium recovery (>75%) in comparison to the control (68.9%). The highest recovery was attained using SD500 (87.0%), followed by MP500 (86.1%). These values are slightly lower than the results reported by Muhmood et al. (2019) for nutrient recovery as struvite using wheat straw (93.9%) and rice husk biochar (91.5%), at a pH of 9.5; yet the recovery values were higher when magnesium-impregnated ground coffee bean (38.6%) and palm tree trunk waste biochar (54.8%) were utilized by Zin and Kim. (2021). These variations could also be an outcome of different Mg^{2+}:PO_4^{3-} molar ratios and biochar dosages used in the studies. Considering these outcomes, SD500 was chosen as the most optimum biochar type for struvite crystallization, in addition to the difference in the relative crystal size.

Dosage optimization was carried out for SD500 biochar considering struvite yield, phosphate and ammonium recovery, and relative crystal size as desirable outcomes (Table 3). Struvite yield (8.12 g L^{-1}) increased

Table 3
Effect of biochar dosage on struvite crystallization by seeding of optimum biochar type (Sawdust500) (Data are summerized as mean ± standard deviation).

Sawdust500 dosage (g L^{-1})	Struvite yield (g L^{-1})	PO_4^{3-} recovery (%)	NH_4^+ recovery (%)	Relative crystal size difference (%)
0	4.07 ± 1.09	80.5 ± 1.5	68.9 ± 4.7	–
0.5	7.34 ± 0.89	91.4 ± 2.0	86.3 ± 0.7	75.1 ± 1.1
1.0	7.91 ± 1.93	97.8 ± 1.6	87.0 ± 1.5	85.1 ± 2.0
1.5	8.08 ± 0.53	98.2 ± 0.9	89.1 ± 1.4	86.1 ± 0.7
2.0	8.12 ± 1.48	97.9 ± 0.2	89.0 ± 3.5	88.7 ± 0.6

(The dosage effects were statistically significant for struvite yield, PO_4^{3-} recovery and NH_4^+ recovery).

with biochar dosage compared to the non-seeded treatment (4.07 g L^{-1}) and was recorded as highest for 2 g L^{-1} as increasing the dosage can provide more active sites for crystal growth and secondary nucleation (Frawley et al., 2012). Phosphate recovery was highest (98.2%) for the 1.5 g L^{-1} dosage, which was ~20% greater than the non-seeded treatment (80.5%). Although 1.5 g L^{-1} seems to be the optimum, considering the minor differences in the outcomes and biochar dosage required, 1 g L^{-1} was the economical and optimum choice for achieving higher struvite recovery and crystal size. In a similar study, higher phosphate and ammonium recoveries were obtained with 0.75 g L^{-1} of wheat straw biochar and rice husk biochar, and only a negligible difference beyond this dosage was noticed (Muhmood et al., 2019). In a pilot-scale study, 0.5 g L^{-1} mealworm frass biochar was used as the optimum dosage for struvite precipitation (Wang et al., 2022).

3.3. Effects of biochar on struvite crystallization: feedstock type and pyrolysis temperature

Regardless of the feedstock, pH and EC show a positive correlation to struvite yield, except for a neutral correlation in the case of sawdust (Fig. 3). However, its influence on the outcomes was negligible due to buffering effect. Ash content of biochars had a positive correlation with struvite yield, except for sawdust and manure pellet. Though the direct influence of ash content on struvite yield is unknown, its indirect effect through surface area and pore volume is reported in the literature (Ronsse et al., 2013). Irrespective of the feedstock, surface area and pore volume had positively contributed to struvite yield, especially in the case of SD. Seeding materials with higher surface area and porosity have been reported to improve nutrient recovery and struvite crystal size

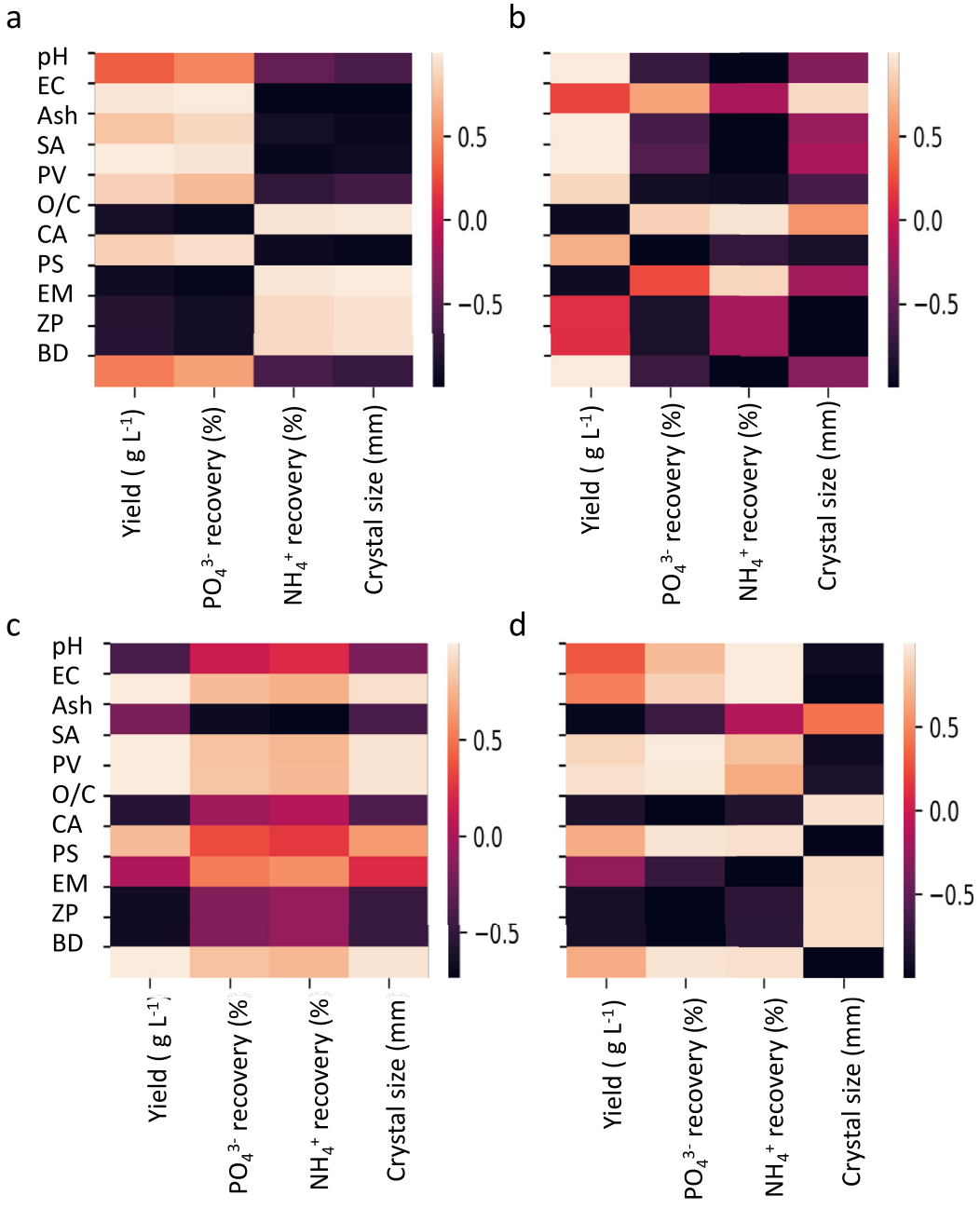

Fig. 3. Pearson correlation showing the effect of biochar properties on struvite recovery with respect to different feedstock types a) canola straw, b) wheat straw, c) sawdust and d) manure pellets (EC: Electrical conductivity (mS cm^{-1}); Ash: Ash content (%); SA: Surface area (m^2 g^{-1}); PV: Pore volume (cm^3 g^{-1}); O/C: Oxygen: Carbon ratio; CA: Contact angle (°); PS: Particle size (mm); EM: Electrophoretic mobility (μm. Cm Vs^{-1}); ZP: Zeta potential (mV) and BD: Bulk density (g cm^{-3})).

(Muhmood et al., 2019). Surface area can also improve the secondary nucleation process occurring on the surface of seeds (Frawley et al., 2012). However, minor discrepancies can be observed with the influence of surface area and pore volume on struvite crystal size, which could be because of the lack of data linearity due to uncertain condensation and the devolatilization of microwave heating.

In the case of bulk properties, an increase in bulk density favored struvite yield for all given feedstocks. However, it had a negative correlation with struvite crystal size, except for SD. Larger particle size suppressed struvite yield for every feedstock due to lower surface area. Also, particles with larger sizes settle down faster, allowing only the binding of struvite crystals but preventing further crystal growth. Yet, a positive correlation between biochar particle size and struvite crystal size can be seen for canola straw biochar, as the average particle size was higher, which could have contributed to the overall crystal size. Though bulk density was very high in manure pellet biochar, smaller particle sizes assisted in the struvite recovery process. Therefore, a balance between bulk density and particle size should be struck to enhance crystallization and nutrient recovery.

As far as suspension properties are concerned, a higher contact angle and lower O/C ratio indicate higher hydrophobicity (Hassan et al., 2020; Adhikari et al., 2022), which explains their positive and negative correlation with struvite yield for a given feedstock (Fig. 3). The wheat straw biochar showed a negative influence on phosphate and ammonium recovery and struvite crystal size due to the superhydrophobic nature of WS500. Only sawdust exhibited a progressive effect on crystal size, which gives an idea of the optimum hydrophobicity of the biochar required for crystallization; however, the effect of temperature should be analyzed to gain more insights. With respect to the electrokinetic properties, the negative correlation indicated that a decrease in zeta potential and electrophoretic mobility increases struvite yield for a given feedstock. This is advantageous for seeding as lower zeta potential, and electrophoretic mobility signify particle stability (Yang et al., 2022).

As the temperature increased from 300 to 500 °C, the ash content of the biochar increased, shifting the positive correlation with struvite yield to neutral (Fig. 4). Similar relationship between temperature and ash content and its influence on biochar pH has been described in the literature (Tomczyk et al., 2020). Analogous to ash content, biochar's surface area and pore volume also increased with temperature, which could be because of lignin, cellulose, and hemicellulose decomposition and the development of channel structures with temperature. Hence the positive correlation with struvite crystallization outcomes can be seen to increase with temperature (Fig. 4). In general, biochars produced above 400 °C have a higher surface area and micropore structure, which makes them suitable for adsorption-related experiments (Uchimiya et al., 2011). Seeding struvite crystallization using biochar follows a mechanism similar to adsorption where small struvite crystals adsorb/precipitate on the surface of biochar using van der Wall's force to further grow in size (Nageshwari et al., 2022; Li et al., 2016, 2017). Though a clear relationship between bulk density and crystal size cannot be described, higher bulk density seemed to negatively influence crystal size at all pyrolysis temperatures. Similarly, the larger particle size of biochar affected struvite yield, and phosphate and ammonium recovery, except for 400 °C. However, regardless of the temperature, an increase in particle size increased the crystal size of struvite, as the latter was a cumulative measure of the formed biochar-struvite composite.

Though surface hydrophobicity/hydrophilicity is not an unambiguous factor determining particle's adsorption efficiency, it is crucial for particle suspension in a medium. Pyrolysis temperature increased the hydrophobicity of biochar due to the loss of O- and H- containing functional groups and organized carbon layers on the surface. At temperatures >500 °C, biochar exhibited lower ion exchange capacity. Whereas, at temperatures <400 °C, the surface functional groups are more diverse due to aliphatic structures (Tomczyk et al., 2020). It is evident from the influence of contact angle that neither lower nor higher temperature had a significantly positive effect on struvite recovery outcomes (Fig. 4).

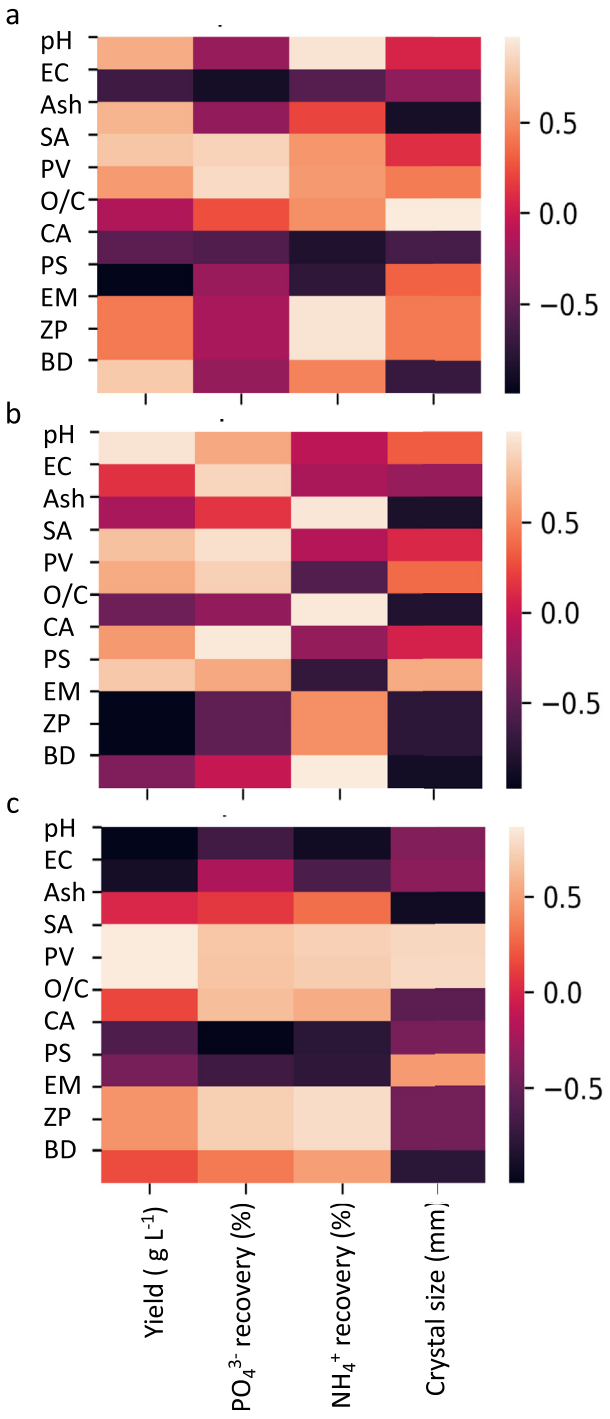

Fig. 4. Pearson correlation showing the effect of biochar properties on struvite recovery with respect to different pyrolysis temperatures a) 300 °C, b) 400 °C and c) 500 °C (EC: Electrical conductivity (mS cm^{-1}); Ash: Ash content (%); SA: Surface area (m^2 g^{-1}); PV: Pore volume (cm^3 g^{-1}); O/C: Oxygen: Carbon ratio; CA: Contact angle (°); PS: Particle size (mm); EM: Electrophoretic mobility (μm. Cm Vs^{-1}); ZP: Zeta potential (mV) and BD: Bulk density (g cm^{-3}).

Higher temperatures offered higher stability for zeta potential and electrophoretic mobility, thereby favouring struvite crystal size.

3.4. Combined influence of biochar properties on struvite crystallization

The correlation centroid obtained through PCA was used to study the relationship between the biochar properties towards struvite crystallization (Fig. S3). F1 and F2 represent principal components (PC) 1 and 2.

The properties/variables that lie close to the x-axis contribute to PC1 and vice versa. In this context, zeta potential (20.8%) > electrophoretic mobility (20.8%) > contact angle (13.8%) > bulk density (9.2%) > O/C ratio (9.0%) in determining PC1, whereas ash content (19.6%) > pore volume (16.3%) > bulk density (15.2%) > surface area (14.4%) > pH (12.7) contributed to PC2. The variables pointed in the same direction are positively correlated with each other as opposed to variables in the diagonal quadrant. Meanwhile, variables placed at right angles are unrelated (no correlation) to each other (Bro and Smilde, 2014). pH, electrical conductivity and contact angle lie in the same quadrant and are positively correlated. These three characteristics depend on the type of functional groups present on the biochar surface. For instance, biochars with aromatic surface functional groups are more hydrophobic. As the temperature increased, aliphatic functional groups were lost and more –OH and aromatic functional groups were formed, which further increased the pH of biochar (Hassan et al., 2020).

The ash content and bulk density were positively correlated with each other but were not correlated with pH, electrical conductivity or contact angle in the adjacent quadrant. Manure pellet biochars produced at different pyrolytic temperatures can be seen to be placed around ash content and bulk density due to their higher values (Fig. S4). Biochar particle size had a negative correlation with the bulk density of biochar. Frawley et al. (2012) reported that a direct relationship between biochar particle size and surface area, and pore volume could be observed, as smaller particles have a higher surface area and porosity. On the contrary, higher inorganic mineral content (ash content) in biochar negatively correlated with surface area and pore volume. This occurs due to the inorganic elements' blockage or filling of micropores on biochar surfaces (Ronsee et al., 2013). However, surface area and pore volume are positively correlated with each other and placed close to SD500 in the loading plot, confirming its performance towards struvite crystallization (Fig. S4). The electrokinetic properties, such as zeta potential and electrophoretic mobility, are very closely associated with each other, as represented by the same variable line. They are present at an obtuse angle with particle size, pH and electrical conductivity, indicating a negative correlation.

4. Conclusions

Feedstock type and MAP temperature significantly impacted biochar properties and, thus their seed characteristics for struvite crystallization. Though SD500 performed better, MP500 also achieved comparable yields due to higher surface area and hydrophobicity, and its inorganic content is an added advantage considering fertilizing applications. Biochars with high surface area, pore volume and stability are best suited for seeding struvite crystallization. However, a larger dataset will help us understand the influence of other variables better. Using ununiform biochar particle size was a drawback in this study; overcoming this will reflect its role in struvite recovery well. In addition, further investigation on the nutrient value of biochar obtained from different feedstocks and their ability to adsorb other nutrients in the medium can be of potential interest for fertilizer applications.

Declaration of competing interest

The authors declare that they have no known competing financial interests or personal relationships that could have appeared to influence the work reported in this paper.

Acknowledgements

The authors thank the Department of Renewable Resources, the University of Alberta, for providing the necessary research facility. We greatly acknowledge the Overseas Visiting Doctoral Fellowship (OVDF) from the Science and Engineering Research Board (SERB), Government of India for funding the first author and the Natural Science and Engineering Research Council (NSERC, grant # RGPIN-2018-05700) of Canada for supporting this research. We also would like to thank Prof. Lena Ma and the anonymous reviewers for their constructive comments on a previous version of the manuscript.

Appendix A. Supplementary data

Supplementary data to this article can be found online at https://doi.org/10.1016/j.seh.2023.100015.

References

Adhikari, S., Timms, W., Mahmud, M.P., 2022. Optimising water holding capacity and hydrophobicity of biochar for soil amendment–a review. Sci. Total Environ., 158043
Battistoni, P., Pavan, P., Prisciandaro, M., Cecchi, F., 2000. Struvite crystallization: a feasible and reliable way to fix phosphorus in anaerobic supernatants. Water Res. 34 (11), 3033–3041.
Bro, R., Smilde, A.K., 2014. Principal component analysis. Anal. Methods 6 (9), 2812–2831.
Chen, W., Ding, S., Lin, Z., Peng, Y., Ni, J., 2020. Different effects of N2-flow and air-limited pyrolysis on bamboo-derived biochars' nitrogen and phosphorus release and sorption characteristics. Sci. Total Environ. 711, 134828.
Claoston, N., Samsuri, A.W., Ahmad Husni, M.H., Mohd Amran, M.S., 2014. Effects of pyrolysis temperature on the physicochemical properties of empty fruit bunch and rice husk biochars. Waste Manag. Res. 32 (4), 331–339.
Fidel, R.B., Laird, D.A., Thompson, M.L., Lawrinenko, M., 2017. Characterization and quantification of biochar alkalinity. Chemosphere 167, 367–373.
Foong, S.Y., Liew, R.K., Yang, Y., Cheng, Y.W., Yek, P.N.Y., Mahari, W.A.W., Lee, X.Y., Han, C.S., Vo, D.N., Le, Q.V., Aghbashlo, M., Tabatabaei, M., Sonne, C., Peng, W., Lam, S.S., 2020. Valorization of biomass waste to engineered activated biochar by microwave pyrolysis: progress, challenges, and future directions. Chem. Eng. J. 389, 124401.
Frawley, P.J., Mitchell, N.A., Ó'Ciardhá, C.T., Hutton, K.W., 2012. The effects of supersaturation, temperature, agitation and seed surface area on the secondary nucleation of paracetamol in ethanol solutions. Chem. Eng. Sci. 75, 183–197.
Gabhi, R., Basile, L., Kirk, D.W., Giorcelli, M., Tagliaferro, A., Jia, C.Q., 2020. Electrical conductivity of wood biochar monoliths and its dependence on pyrolysis temperature. Biochar 2 (3), 369–378.
Hassan, M., Liu, Y., Naidu, R., Parikh, S.J., Du, J., Qi, F., Willett, I.R., 2020. Influences of feedstock sources and pyrolysis temperature on the properties of biochar and functionality as adsorbents: a meta-analysis. Sci. Total Environ. 744, 140714.
Hu, P., Zhang, Y., Liu, L., Wang, X., Luan, X., Ma, X., Chu, P.K., Zhou, J., Zhao, P., 2019. Biochar/struvite composite as a novel potential material for slow release of N and P. Environ. Sci. Pollut. Control Ser. 26 (17), 17152–17162.
Huang, Y.F., Chiueh, P.T., Shih, C.H., Lo, S.L., Sun, L., Zhong, Y., Qiu, C., 2015. Microwave pyrolysis of rice straw to produce biochar as an adsorbent for CO2 capture. Energy 84, 75–82.
Kataki, S., West, H., Clarke, M., Baruah, D.C., 2016. Phosphorus recovery as struvite: recent concerns for use of seed, alternative Mg source, nitrogen conservation and fertilizer potential. Resour. Conserv. Recycl. 107, 142–156.
Krishnamoorthy, N., Dey, B., Arunachalam, T., Paramasivan, B., 2020. Effect of storage on physicochemical characteristics of urine for phosphate and ammonium recovery as struvite. Int. Biodeterior. Biodegrad. 153, 105053.
Krishnamoorthy, N., Dey, B., Unpaprom, Y., Ramaraj, R., Maniam, G.P., Govindan, N., Jayaraman, S., Arunachalam, T., Paramasivan, B., 2021. Engineering principles and process designs for phosphorus recovery as struvite: a comprehensive review. J. Environ. Chem. Eng. 9 (5), 105579.
Kwak, J.H., Islam, M.S., Wang, S., Messele, S.A., Naeth, M.A., El-Din, M.G., Chang, S.X., 2019. Biochar properties and lead (II) adsorption capacity depend on feedstock type, pyrolysis temperature, and steam activation. Chemosphere 231, 393–404.
Li, R., Wang, J.J., Zhou, B., Awasthi, M.K., Ali, A., Zhang, Z., Mahar, A., 2016. Recovery of phosphate from aqueous solution by magnesium oxide decorated magnetic biochar and its potential as phosphate-based fertilizer substitute. Bioresour. Technol. 215, 209–214.
Li, R., Wang, J.J., Zhou, B., Zhang, Z., Liu, S., Lei, S., Xiao, R., 2017. Simultaneous capture removal of phosphate, ammonium and organic substances by MgO impregnated biochar and its potential use in swine wastewater treatment. J. Clean. Prod. 147, 96–107.
Liao, M., Liu, Y., Tian, E., Ma, W., Liu, H., 2020. Phosphorous removal and high-purity struvite recovery from hydrolyzed urine with spontaneous electricity production in Mg-air fuel cell. Chem. Eng. J. 391, 123517.
Liu, Y., Rahman, M.M., Kwag, J.H., Kim, J.H., Ra, C.S., 2011. Eco-friendly production of maize using struvite recovered from swine wastewater as a sustainable fertilizer source. Asian-Australas. J. Anim. Sci. 24 (12), 1699–1705.
Liu, Z., Zhao, Q., Lee, D.J., Yang, N., 2008. Enhancing phosphorus recovery by a new internal recycle seeding MAP reactor. Bioresour. Technol. 99 (14), 6488–6493.
Muhmood, A., Lu, J., Kadam, R., Dong, R., Guo, J., Wu, S., 2019. Biochar seeding promotes struvite formation, but accelerates heavy metal accumulation. Sci. Total Environ. 652, 623–632.
Murphy, J.A.M.E.S., Riley, J.P., 1962. A modified single solution method for the determination of phosphate in natural waters. Analytica Chimica Acta 27, 31–36.

Nageshwari, K., Chang, S.X., Balasubramanian, P., 2022a. Integrated electrocoagulation-flotation of microalgae to produce Mg-laden microalgal biochar for seeding struvite crystallization. Sci. Rep. 12 (1), 11463.
Nzediegwu, C., Arshad, M., Ulah, A., Naeth, M.A., Chang, S.X., 2021. Fuel, thermal and surface properties of microwave-pyrolyzed biochars depend on feedstock type and pyrolysis temperature. Bioresour. Technol. 320, 124282.
Nzediegwu, C., Naeth, M.A., Chang, S.X., 2022. Feedstock type drives surface property, demineralization and element leaching of nitric acid-activated biochars more than pyrolysis temperature. Bioresour. Technol. 344, 126316.
Prabhu, K., Malode, S.J., Veerapur, R.S., Shetti, N.P., 2021. Clay-based carbon sensor for electro-oxidation of nimesulide. Mater. Chem. Phys. 272, 124992.
Robinson Junior, N.A., Wu, S.X., Zhu, J., Zhan, Y., 2022. Optimization of a dual-chamber electrolytic reactor with a magnesium anode and characterization of struvite produced from synthetic wastewater. Environ. Technol. 1–37.
Ronsse, F., Van Hecke, S., Dickinson, D., Prins, W., 2013. Production and characterization of slow pyrolysis biochar: influence of feedstock type and pyrolysis conditions. Gcb Bioenergy 5 (2), 104–115.
Stella Mary, G., Sugumaran, P., Niveditha, S., Ramalakshmi, B., Ravichandran, P., Seshadri, S., 2016. Production, characterization and evaluation of biochar from pod (Pisum sativum), leaf (Brassica oleracea) and peel (Citrus sinensis) wastes. Int. J. Recycl. Org. Waste Agric. 5 (1), 43–53.
Tarragó, E., Puig, S., Ruscalleda, M., Balaguer, M.D., Colprim, J., 2016. Controlling struvite particles' size using the up-flow velocity. Chem. Eng. J. 302, 819–827.
Tomczyk, A., Sokołowska, Z., Boguta, P., 2020. Biochar physicochemical properties: pyrolysis temperature and feedstock kind effects. Rev. Environ. Sci. Biotechnol. 19 (1), 191–215.
Uchimiya, M., Wartelle, L.H., Klasson, K.T., Fortier, C.A., Lima, I.M., 2011. Influence of pyrolysis temperature on biochar property and function as a heavy metal sorbent in soil. J. Agric. Food Chem. 59 (6), 2501–2510.
Wallace, C.A., Afzal, M.T., Saha, G.C., 2019. Effect of feedstock and microwave pyrolysis temperature on physio-chemical and nano-scale mechanical properties of biochar. Bioresources and Bioprocessing 6 (1), 1–11.
Wang, S., Sun, K., Xiang, H., Zhao, Z., Shi, Y., Su, L., Tan, C., Zhang, L., 2022. Biochar-seeded struvite precipitation for simultaneous nutrient recovery and chemical oxygen demand removal in leachate: from laboratory to pilot scale. Front. Chem. 10.
Xu, C.Y., Li, Q.R., Geng, Z.C., Hu, F.N., Zhao, S.W., 2020. Surface properties and suspension stability of low-temperature pyrolyzed biochar nanoparticles: effects of solution chemistry and feedstock sources. Chemosphere 259, 127510.
Xu, G., Zhang, Y., Shao, H., Sun, J., 2016. Pyrolysis temperature affects phosphorus transformation in biochar: chemical fractionation and 31P NMR analysis. Sci. Total Environ. 569, 65–72.
Yang, W., Li, B., Shang, J., 2022. Aggregation kinetics of biochar nanoparticles in aqueous environment: interplays of anion type and bovine serum albumin. Sci. Total Environ. 833, 155148.
Yu, R., Geng, J., Ren, H., Wang, Y., Xu, K., 2013. Struvite pyrolysate recycling combined with dry pyrolysis for ammonium removal from wastewater. Bioresour. Technol. 132, 154–159.
Zhang, Y., Fan, S., Liu, T., Fu, W., Li, B., 2022. A review of biochar prepared by microwave-assisted pyrolysis of organic wastes. Sustain. Energy Technol. Assessments 50, 101873.
Zin, M.M.T., Kim, D.J., 2021. Simultaneous recovery of phosphorus and nitrogen from sewage sludge ash and food wastewater as struvite by Mg-biochar. J. Hazard Mater. 403, 123704.